

# *LiDAR mapping of tidal marshes for ecogeomorphological modelling in the TIDE project*

Conference or Workshop Item

Accepted Version

Mason, D. C., Marani, M., Belluco, E., Feola, A., Ferrari, S., Katzenbeisser, R., Lohani, B., Menenti, M., Paterson, D.M., Scott, T.R., Vardy, S., Wang, C. and Wang, H.-J. (2005) LiDAR mapping of tidal marshes for ecogeomorphological modelling in the TIDE project. In: Eighth International Conference on Remote Sensing for Marine and Coastal Environments, 17-19 May 2005, Halifax, Nova Scotia. (Unpublished) Available at <http://centaur.reading.ac.uk/5887/>

It is advisable to refer to the publisher's version if you intend to cite from the work. See [Guidance on citing](#).

including copyright law. Copyright and IPR is retained by the creators or other copyright holders. Terms and conditions for use of this material are defined in the [End User Agreement](#).

[www.reading.ac.uk/centaur](http://www.reading.ac.uk/centaur)

## **CentAUR**

Central Archive at the University of Reading

Reading's research outputs online

# LIDAR MAPPING OF TIDAL MARSHES FOR ECOGEOMORPHOLOGICAL MODELLING IN THE TIDE PROJECT\*

D. C. Mason<sup>1</sup>, M. Marani<sup>2</sup>, E. Belluco<sup>2</sup>, A. Feola<sup>2</sup>, S. Ferrari<sup>2</sup>, R. Katzenbeisser<sup>3</sup>, B. Lohani<sup>4</sup>,  
M. Menenti<sup>5</sup>, D. M. Paterson<sup>6</sup>, T.R. Scott<sup>1</sup>, S. Vardy<sup>6</sup>, C. Wang<sup>5</sup> and H-J. Wang<sup>1</sup>.

<sup>1</sup>ESSC, University of Reading, UK

<sup>2</sup>International Center for Hydrology 'D. Tonini', University of Padua, Italy

<sup>3</sup>TopoSys GmbH, Biberach, Germany

<sup>4</sup>Indian Institute of Technology, Kanpur, India

<sup>5</sup>LSIIT, Universite Louis Pasteur, Strasbourg, France

<sup>6</sup>Gatty Marine Laboratory, University of St. Andrews, UK

## ABSTRACT

The European research project TIDE (Tidal Inlets Dynamics and Environment) is developing and validating coupled models describing the morphological, biological and ecological evolution of tidal environments. The interactions between the physical and biological processes occurring in these regions requires that the system be studied as a whole rather than as separate parts. Extensive use of remote sensing including LiDAR is being made to provide validation data for the modelling. This paper describes the different uses of LiDAR within the project and their relevance to the TIDE science objectives. LiDAR elevation accuracy at each site has been evaluated using ground reference data acquired with differential GPS. Estimation of the heights of the short and sparse vegetation on marshes is being investigated by analysis of the statistical distribution of the measured LiDAR heights. A semi-automatic technique has been developed to extract tidal channel networks from LiDAR data either used alone or fused with aerial photography.

## 1.0 INTRODUCTION

The TIDE project is attempting to develop ecogeomorphological models of the inter-tidal zone in which the models describing the physical, biological and ecological processes occurring in this complex environment are coupled together to reflect the interactions that occur between these processes (Marani et al., 2004). Sediment transport in the inter-tidal zone, while forced mainly by the hydrodynamics, is also dependent on biological and ecological factors. The zone may be colonised by halophytic vegetation and sediment microbial assemblages (microphytobenthos) that may stabilise and trap the sediments. In turn, the dynamics of this ecology will be influenced by the sediment transport regime. The interplay between these factors will govern whether accretion occurs and a marsh stabilises, or whether erosive effects dominate (Allen, 2000).

The inter-tidal zone possesses a complex topography dissected by networks of tidal channels. The topography is one of a number of factors controlling the spatial distribution of the biota in the zone. The observed characteristics of the zone form the validation data to which the models must conform. The modelling requires observations to be made at small spatial scales and over relatively large areas, and to

---

\* Presented at the Eighth International Conference on Remote Sensing for Marine and Coastal Environments, Halifax, Nova Scotia, 17-19 May 2005.

be repeated at intervals ranging from days to years. These requirements have been met using remotely sensed data. Multispectral data have been gathered by aircraft, satellite and balloon, and elevation data by LiDAR. LiDAR is able to provide topographic data at a scale and height accuracy that matches that required to study features such as networks and vegetation structure, as well as that of the multispectral data. The availability of LiDAR is likely to be significant for the study of inter-tidal geomorphology, as one reason that research on this topic has lagged behind that of fluvial geomorphology has been the difficulty of obtaining sufficiently dense and accurate DTMs of inter-tidal zones. TIDE LiDAR data have been acquired from three coastal environments having different tidal regimes, the Venice Lagoon in Italy, Morecambe Bay in England, and the Eden estuary in Scotland. The data of the Venice Lagoon were acquired by the TopoSys FALCON II LiDAR, whilst the data of Morecambe Bay and the Eden were acquired by the Optech ALTM 2033 LiDAR owned by the UK Environment Agency. Two flights were made over the Venice Lagoon, one over Morecambe Bay and three over the Eden estuary. LiDAR has been used for three main purposes in TIDE –

- 1) The production of inter-tidal DTMs for use in modelling inter-tidal hydrodynamics and in studying the geomorphology of channel networks,
- 2) In conjunction with multispectral data, the classification of the short sparse marsh vegetation using the statistics of measured elevations within a local area to deduce the average height and dominant type of vegetation;
- 3) In conjunction with co-registered vegetation classifications from hyperspectral and multispectral data, the identification of characteristic elevation ranges defining optimal edaphic conditions for each vegetation species.

## 2.0 VALIDATION OF LIDAR ELEVATIONS

In order to evaluate the accuracy of the LiDAR elevation estimates acquired for Venice salt-marshes, more than 200 GPS observations were performed and post-processed to obtain estimation uncertainties smaller than 1 cm in all three co-ordinate directions. The GPS reference observations were performed randomly throughout the San Felice salt marsh, one of the main TIDE study sites (e.g. Marani et al., 2004 for a detailed description of the site). For the purpose of validation we consider here LiDAR raw data, i.e. the set of  $(x,y,z)$  values obtained from each laser return and relative to a footprint of about 45 cm. LiDAR data were projected onto the same reference system used for GPS observations (UTM-WGS84 zone 33). In order to allow a one-to-one comparison between LiDAR and GPS estimates, each GPS observation, say  $z_i^G$ , was associated to the nearest LiDAR value,  $z_i^L$ . Because the co-registration of LiDAR and GPS observations is inevitably imperfect, mainly due to uncertainties in airplane positioning, we sought to improve it by determining an ‘optimal’ displacement,  $(\Delta x, \Delta y)$ , to be applied to LiDAR observations in order to minimize the square error  $\sum_i (z_i^G - z_i^L)^2$ . Notice that such error depends on  $(\Delta x, \Delta y)$  through the effects that the displacement has on the association of GPS and LiDAR estimates,  $(z_i^G, z_i^L)$ , determined through the above nearest-neighbour criterion. The ‘optimal’ displacement was then applied to all  $(x,y)$  co-ordinates of LiDAR observations and the final, most correlated, couples  $(z_i^G, z_i^L)$  were considered.

The comparison of surface elevation estimates,  $(z_i^G, z_i^L)$ , obtained through this procedure is shown in figure 1. The observed GPS-LiDAR relationship may be considered as approximately linear ( $R^2=0.50$ ), with a slope smaller than one, indicating that LiDAR observations tend to overestimate actual elevation and that the errors tend to increase with elevation. This effect is likely due to the variable height and density of salt-marsh vegetation, which, in the Venice lagoon, increases with soil elevation. Notice that all salt-marsh vegetation species are shorter than 50 cm, and thus below the threshold which produces two distinct returns from the same sampling point (approx. 2 m). Nevertheless, though the vegetation is not tall

enough to cause two distinct laser returns, the single return detected does not seem to be coming from the soil, but from an elevation located between the soil and the top of the canopy. The increasing LiDAR overestimation with soil elevation may thus be explained by considering that for the more elevated sites of the marsh, where vegetation is denser and taller, the probability that the laser return observed by the sensor comes from near the canopy top increases. The square-root errors computed in the vertical direction as the mean square difference between GPS observations and the regression line are  $\sigma_e = 0.06$  m. The correction of LiDAR observations through the regression line thus provides improved estimates of soil elevation with an average error smaller than 6 cm.

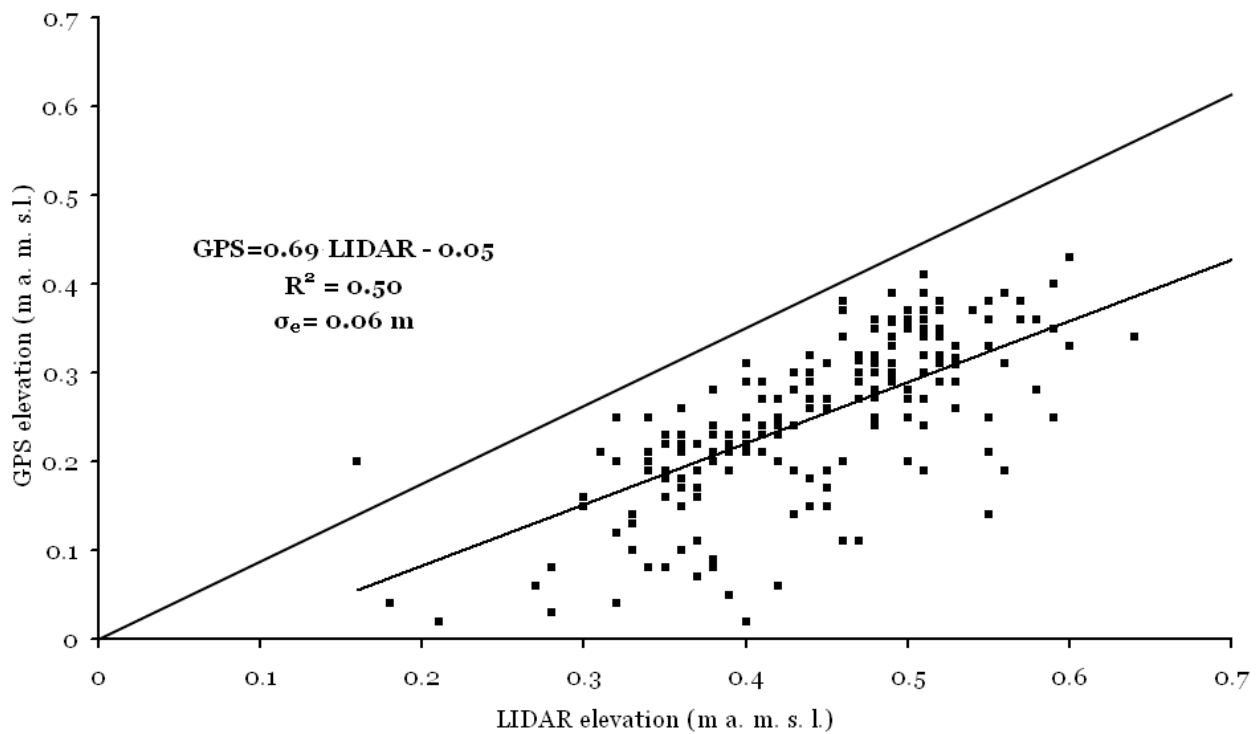


Figure 1. Comparison between LiDAR Raw Data Elevation Estimates and GPS Reference Observations for a Set of more than 200 sites throughout the San Felice Salt Marsh, Venice Lagoon .

### 3.0 ANALYSIS OF LIDAR MEASUREMENTS

The procedure developed during the project to analyse LIDAR data aims at providing estimates of low vegetation height, namely lower than the smallest observable difference between the first and the last detected return from the same location on the ground. The procedure relies on the principle that the waveform of the backscatter signal depends on the vertical distribution of leaves within the observed vegetation canopy. The estimated travel time of the laser pulse will then be slightly different according to vegetation height. Local statistics of a sample of LIDAR measurements provide information on canopy architecture and vegetation height.

The procedure as implemented can be applied to samples of 50 to 100 individual laser measurements (raw data) constructed by using a polygon of arbitrary shape or a short segment of a linear

sequence of laser measurements. In either case the reference points need to be geo-located. The frequency distribution of laser measurements in each sample set provides information in different ways:

- difference between maximum observed elevation and ground elevation determined with GPS observations;
- difference between maximum and minimum observed elevation;
- standard deviation of elevation values.

The LIDAR system used to measure surface morphology and elevation does not have the vertical resolution required to measure the height of low vegetation directly, i.e. as the difference between the first and last echo received from the same target. On the other hand the vertical resolution of the raw data provided by the TopoSys LIDAR system, i.e. 0.01 m, is sufficient to observe surface topography in sufficient detail. The problem then becomes to determine local ground elevation and estimate vegetation height as the difference between observed elevation (LIDAR) and the local ground elevation. Two solutions were explored:

- use of independent GPS measurements;
- local statistics of LIDAR observations

The first solution is more accurate, but not viable for the entire study area, while the second relies on the assumption that a local sample ( $1\text{m}^2$  say) of LIDAR observations includes a few “ground hits”, i.e. measurements of elevation relating to the ground rather than to the vegetation above it. Two data sets were used to evaluate these two solutions:

- the observations collected at a number of Region Of Interest polygons (ROI-s) in support of the analysis of the hyperspectral image data;
- measurements of vegetation height and (x,y,z) coordinates at selected points;

Frequency

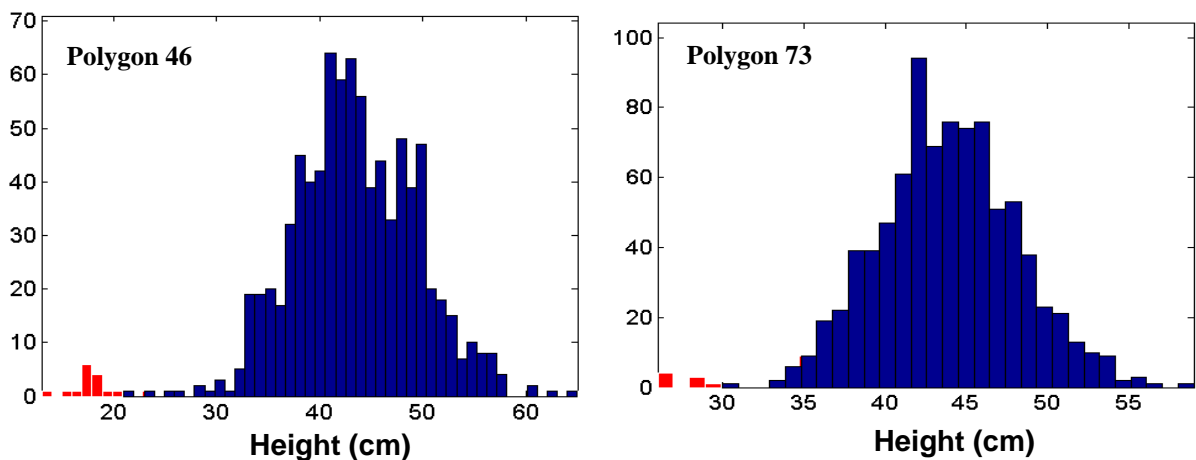


Figure 2. Frequency Distribution of GPS Elevation (red) along the Boundary of ROI no. 46 (a) and no. 73 (b) and of LIDAR Elevation (blue) within each ROI.

For the ROI-s case, all LIDAR measurements within a ROI were extracted from the raw, last-pulse LIDAR data and combined with all the 3D GPS readings taken along the boundary of the ROI. In the case of the point-observations we used a 4 m sample along the closest LIDAR line to the point where

vegetation height and ground elevation were measured. Results are quite positive. The frequency distributions of the LIDAR and GPS measurements for individual ROI-s (see fig. 2) clearly indicate the separation between the vegetation and ground signal and that the lowest tail of the frequency distribution of LIDAR observations relates to ground observations. The latter implies that local ground elevation may be estimated from local statistics of a LIDAR sample.

The procedure has been validated in two ways:

- A. For a set of reference polygons, GPS observations provided the elevation of points along the contour line of the polygon. The mean and maximum GPS elevation was in good agreement with minimum LIDAR elevation in the sample.
- B. A simple simulation model was applied to estimate the expected laser above-ground elevation of a vegetation canopy, given the vertical distribution of leaves within the canopy. The mean values of observed elevation for all reference polygons were in good agreement with simulated elevations, assuming a uniform leaf distribution between the top of plants and the ground surface.

Two uniform leaf vertical distributions were simulated within layers of different thickness: a) one standard deviation of plant height; b) entire plant height. Simulated LIDAR observations agreed with actual observations for case (b) only (fig. 3).

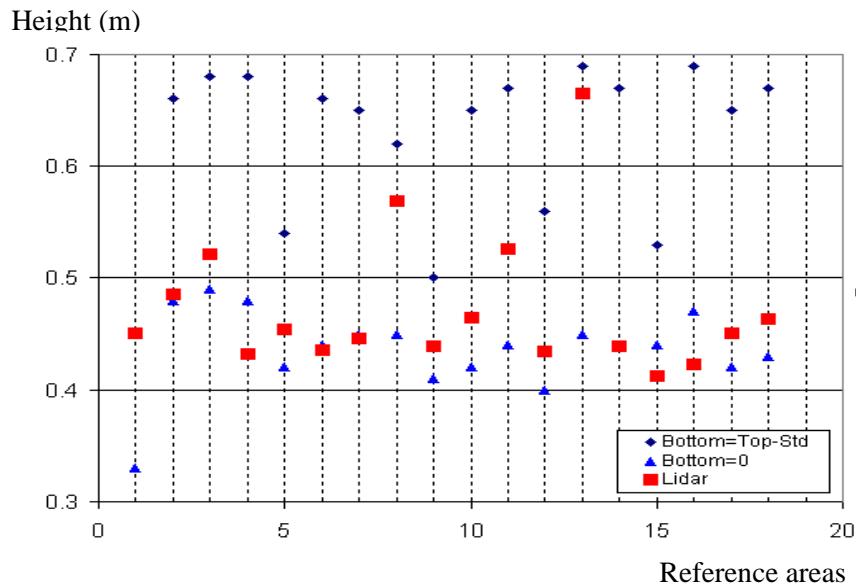


Figure 3. Simulated and Observed LIDAR Vegetation Height (elevation above ground) for 20 Reference Areas; Saltmarsh Venice lagoon, 2002.

The procedure can also be applied to refine maps of ground elevation by re-sampling a map of uncorrected elevation data, with the corrected elevation set equal to the minimum elevation in a sample of uncorrected data. Samples are constructed by running a box filter through the uncorrected data.

#### 4.0 EXTRACTION OF TIDAL CHANNEL NETWORKS

Tidal channel networks are integral features of the inter-tidal zone, and play a key role in tidal propagation, sediment transport and the evolution of tidal flats and salt marshes. The processes governing network development and evolution are currently an open question, and a number of theories are being investigated. Extensive observational data extracted from accurate measurements over large areas of inter-tidal zone are required to validate these theories. The conventional method of measuring networks often involves network planforms being digitised manually from aerial photographs then amended by field survey. In addition field survey of channel cross-sections may be made for a selected subset of channels. The conventional technique, relying heavily on manual intervention, involves a great deal of effort, is somewhat subjective, and can only acquire a limited set of field measurements. Channel dimensions range from several tens of metres wide and several metres deep near the low water mark to only about 30cm wide and 30cm deep for the smallest channels on the marshes. As a spatial resolution of 25cm or so is currently possible with LiDAR, this is able to detect even the smallest channels. The current trend is to acquire LiDAR in conjunction with colour aerial photography or multispectral linescanner data to provide the user with a visual image of the LiDAR DEM. TopoSys LiDAR and linescanner images of part of the Venice lagoon (both 0.5m pixel size) are shown in figure 4.

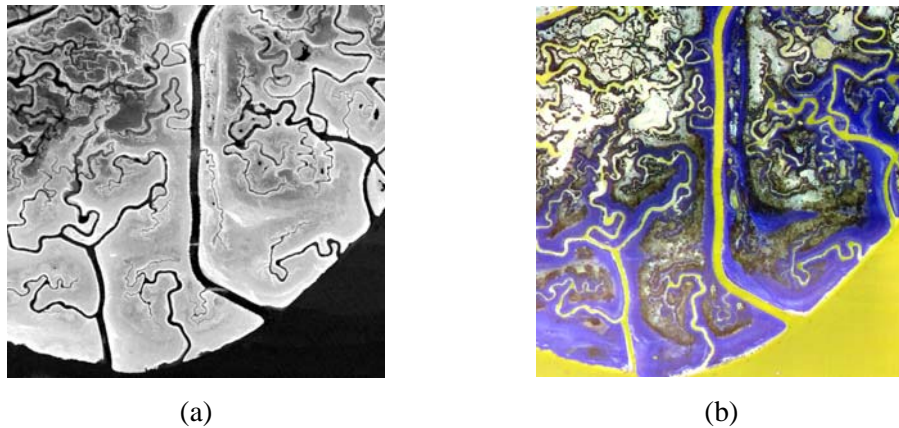


Figure 4. (a) LiDAR Image of the San Felice Marsh in the Venice Lagoon, (b) Linescanner Image.

##### 4.1 CHANNEL EXTRACTION FROM LIDAR DATA

A semi-automatic technique has been developed to extract networks from LiDAR data (Mason and Scott, 2004; Mason et al., submitted). The method is termed semi-automatic because at various points in the procedure the human operator is called upon for assistance, including the correction of errors in the final output. A multi-level knowledge-based approach has been implemented, whereby low level algorithms first extract channel fragments based mainly on image properties then a high level processing stage repairs breaks in the network using domain knowledge.

Edges are first detected in the height image using a multiscale edge detector. Edges that are non-maxima along an axis perpendicular to their edge direction are suppressed. Surviving edge maxima are then thresholded using hysteresis thresholding and thinned to single pixel width. Edge detection of a tidal



channel will generate two anti-parallel edges from either side of it, which must be associated together. This is achieved by generating the distance transform of the edge image, in which a pixel's value is its distance from the nearest edge, with distances being zero at edge pixels. The transform is operated upon to identify positions having distances that are maxima or saddle points, by performing non-maximum suppression followed by thinning. The distance maxima occur at the centrelines of channels, but other maxima of no interest will occur between channels. To differentiate between these two classes, a score is calculated for each maximum. A distance maximum's score is big if it is linked with perfectly anti-parallel edges with a narrow separation bounding runs of pixels with heights less than the edge heights, and with heights increasing away from the channel centre. Long connected strings of pixels having high scores are then selected using hysteresis thresholding.

Breaks in the networks are repaired by extending channel ends in the direction of their ends to join with nearby channels. For each endpoint, a search for a channel centreline pixel to join with is made by searching forward in a triangle with its apex at the endpoint being considered, and oriented in the direction of the endpoint. Domain knowledge is used at this stage, namely that flow paths should proceed downhill. For each candidate centreline pixel in the search triangle, the optimum path along which to join candidate and endpoint is determined using a valley-seeking algorithm. The repaired centreline image is finally converted to one of bankfull channel extents by expanding the channels to their positions of maximum negative curvature.

The channels automatically delineated from figure 4a were validated by comparing them with a set of manually-delineated channels (figure 5a - white = correctly identified channels, red = error of omission, green = error of commission). While the error of omission was low (14%), there was a significant error of commission (42%), due partly to the confusing situation in the NW of the image where the channel structure becomes ambiguous.

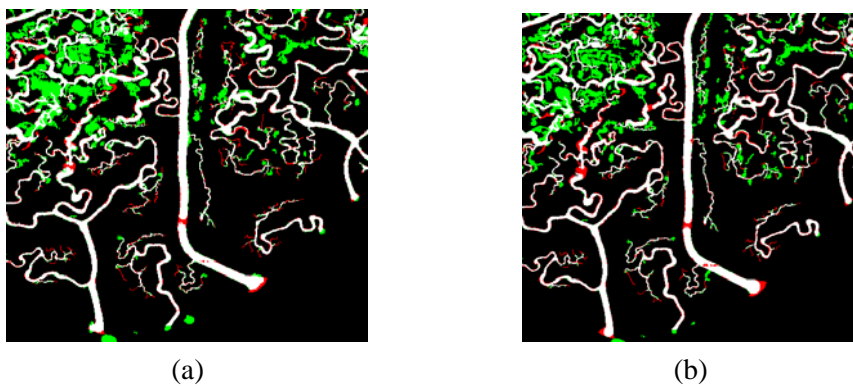


Figure 5. Comparison of Automatic Channel Network Extraction Results and Validation Data (a) Weight  $w = 0$  (LiDAR only), (b)  $w = 0.3$ .

#### 4.2 CHANNEL EXTRACTION FROM FUSED LIDAR AND LINESCANNER DATA

Modern LiDAR data are often acquired in conjunction with simultaneous digital aerial photography/linescanner data, so that the channel extraction algorithm may have a higher signal-to-noise ratio using LiDAR together with linescanner data than from LiDAR alone. Fusion of TopoSys linescanner data (figure 4b) and the LiDAR data from the Venice Lagoon (figure 4a) were considered as an example

(Lohani et al., submitted). The linescanner data consist of four spectral bands, red, green, blue and near-infrared, and are geometrically registered to the LiDAR data. It is apparent from figure 4 that the LiDAR data have a higher signal-to-noise ratio for channels than the linescanner data. The latter have more noise edges (i.e. not from channels) than the LiDAR, but it is difficult to see channel edges in the linescanner data that are not also present in the LiDAR.

The algorithm for channel extraction from LiDAR data was adapted to cope with fused data sets. This involves knowledge-based fusion being carried out at the feature level, with edges from the LiDAR and colour images being combined just after the edge extraction stage. The LiDAR edges are subjected to non-maximum suppression before being combined with the colour edge image. However, the colour edges do not undergo this process to allow for the fact that the colour edge maxima may not occur exactly in the same places as the LiDAR edge maxima. Because the LiDAR appears to give the better signal-to-noise ratio for channel detection, most of the weight is assigned to the LiDAR edges. Also, if the LiDAR edge strength is too small, no edge is detected irrespective of the strength of the corresponding colour edge. After the edges are combined, the algorithm follows that for the LiDAR data alone, and no further account is taken of the colour image. All the subsequent algorithm stages (e.g. the joining algorithm) work purely on the basis of the LiDAR data.

The results for automatic channel extraction using fused data sets were again compared to the manually-delineated validation data (figure 5b). The main conclusion is that fusion does not seem to help much over simply using the LiDAR data alone for channel extraction. For a relative weighting  $w$  of colour edge to LiDAR edge strength, there is a slight reduction in total error (omission + commission) (49%) for the case  $w = 0.3$  compared to using the LiDAR data alone (51%), but for all other cases the total error increases.

## 5.0 CONCLUSION

It can be seen that the LiDAR data collected in TIDE have been of use for several purposes. Validation of the LiDAR elevations against GPS observations indicates that the average LiDAR return is generated at an elevation between the ground and the top of the canopy. Local statistics from proximal samples of LiDAR measurements, used in conjunction with a LiDAR simulator, have provided information on vegetation height, canopy structure and ground elevation. The procedure for channel extraction from LiDAR data has allowed networks to be identified over large areas using objective criteria and reduces fieldwork requirements, though the resulting networks invariably require some correction. The corrected networks may subsequently be used in geomorphological analyses, for example to describe the drainage patterns induced by networks.

## 6.0 ACKNOWLEDGEMENTS

This work was funded under the EU FP5 project TIDE (EVK3-CT-2001-00064).

## 7.0 REFERENCES

- J.R.L. Allen, "Morphodynamics of Holocene salt marshes: a review sketch from the Atlantic and southern North Sea coasts of Europe." *Quaternary Science Reviews*, **19**, 1155-1231, 2000.
- B. Lohani, D.C. Mason, T.R. Scott and B. Sreenivas, "Identification of tidal channel networks from aerial photographs alone and fused with airborne laser altimetry." *Int. J. Remote Sensing* (submitted).

M. Marani, R. Aspden, E. Belluco, M. Camuffo, A. D'Aplao, J. Korczak, S. Lanzoni, C. McGregor, A. Marani, D.C. Mason, M. Menenti, D. Paterson, A. Quirin, R. Rigon, A. Rinaldo, T.R. Scott, S. Silvestri, S. Vardy, H. Wang, "Observations and ecogeomorphological modelling of tidal environments." *Proceedings of the Italian Congress on Hydraulics and Hydraulic Works*, Trento, Italy, October 2004, 8pp, 2004.

M. Marani, S. Lanzoni, S. Silvestri, and A. Rinaldo, Tidal landforms, patterns of halophytic vegetation and the fate of the lagoon of Venice, *J. Marine Syst.*, vol.51, 191-210, 2004.

D.C. Mason, T.R. Scott and H-J. Wang, "Extraction of tidal channel networks from airborne LiDAR data." *ISPRS J. Photogrammetry and Remote Sensing* (submitted).

D.C. Mason and T.R. Scott, "Remote sensing of tidal channel networks and their relation to vegetation." In *The Ecogeomorphology of Tidal Marshes*, eds. Fagherazzi S, Marani M, Blum L). American Geophysical Union, Coastal and Estuarine Studies 59, 27-46, 2004.